AD-783 479

FLUERICS 36 LARGE-SCALE MODELING OF LAMINAR FLUERIC DEVICES

Chris E. Spyropoulos

Harry Diamond Laboratories
Washington, D. C.

February 1974

The findings in this report are not to be construed as an official Department of the Army position unless so designated by other authorized documents.

Citation of manufacturers' or trade names does not constitute an official indorsement or approval of the use thereof.

Destroy this report when it is no longer needed. Do not return it to the originator.

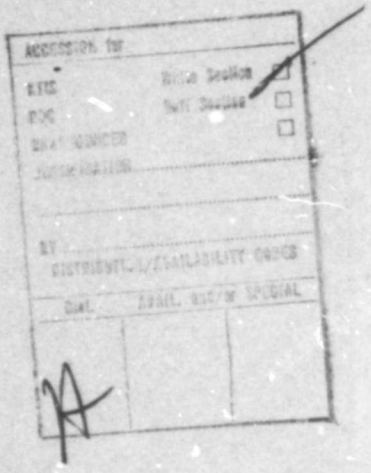

2a

UNCLASSIFIED
SECURITY CLASSIFICATION OF THIS PAGE (When Data Entered)

REPORT DOCUMENTATION PAGE	READ INSTRUCTIONS BEFORE COMPLETING FORM
1. REPORT NUMBER: HDL-TM-73-28	2. GOVT ACCESSION NO.
3. RECIPIENT'S CATALOG NUMBER: AD-783479	
4. TITLE (and Subtitle): FLUERICS 36 LARGE-SCALE MODELING OF LAMINAR FLUERIC DEVICES	5. TYPE OF REPORT & PERIOD COVERED: Technical Memorandum
	6. PERFORMING ORG. REPORT NUMBER
7. AUTHOR(s): CHRIS E. SPYROPOULOS	8. CONTRACT OR GRANT NUMBER(s)
9. PERFORMING ORGANIZATION NAME AND ADDRESS: Harry Diamond Laboratories, Washington, DC 20438	10. PROGRAM ELEMENT, PROJECT, TASK AREA & WORK UNIT NUMBERS: DA-1T61102A33B, Task Area No. 00, Work Unit No. 048A9
11. CONTROLLING OFFICE NAME AND ADDRESS: Commander, HQ Army Materiel Command, 5001 Eisenhower Avenue, Alexandria, Virginia 20315	12. REPORT DATE: February 1974
	13. NUMBER OF PAGES: 29
14. MONITORING AGENCY NAME & ADDRESS(if different from Controlling Office)	15. SECURITY CLASS. (of this report): Unclassified
	15a. DECLASSIFICATION/DOWNGRADING SCHEDULE

16. DISTRIBUTION STATEMENT (of this Report)

APPROVED FOR PUBLIC RELEASE; DISTRIBUTION UNLIMITED

17. DISTRIBUTION STATEMENT (of the abstract entered in Block 20, if different from Report)

18. SUPPLEMENTARY NOTES

AMCMS Code: 611102.11.71200
Project No. 302431

19. KEY WORDS (Continue on reverse side if necessary and identify by block number)

Laminar flow
Liquid modeling
Proportional amplifier

20. ABSTRACT (Continue on reverse side if necessary and identify by block number)

The purpose of this report is to investigate large-scale modeling of laminar flueric flow phenomena. A test facility utilizing silicone oil as the working fluid and Reynolds number as the modeling parameter was designed, constructed, and instrumented. The test facility described is inexpensive and easy to operate. Models can be readily inserted, tested, and modified for retesting. In order to test the validity of modeling, performance characteristics of a large-scale model and an existing laminar-

DD FORM 1 JAN 73 1473 EDITION OF 1 NOV 65 IS OBSOLETE

UNCLASSIFIED
SECURITY CLASSIFICATION OF THIS PAGE (When Data Entered)

air proportional amplifier were compared. Agreement between similar performance characteristics was very good, with differences accounted for by experimental error and the existence of small variation in geometric similarity between the model and air device. Results obtained thus verify that the laws of similitude are valid for the conditions specified, and can be readily used.

TABLE OF CONTENTS

LIST OF ILLUSTRATIONS

LIST OF ILLUSTRATIONS (Cont'd)

LIST OF TABLES

1. INTRODUCTION

The small size of many flueric devices makes it difficult to investigate experimentally internal flow phenomena without significantly interfering with the flow. The complexity of the flow phenomena within flueric devices complicates the task of analytical modeling of these devices. In order to overcome these limitations, investigators utilize large-scale liquid modeling, employing the similarity between air and liquid flow, when the flow is laminar.

In order to investigate quantitatively the flow phenomena in laminar amplifiers and other laminar flueric devices currently under study at the Harry Diamond Laboratories, a test facility was designed, constructed, and instrumented. Silicone oil with a kinematic viscosity of 5.0×10^{-5} m^2/s (50 centistokes) at 25°C was used as the working fluid. The basic test facility is inexpensive and easy to instrument. Models of devices to be tested can be made and modified easily while holding closer percentage tolerances than is practicable with smaller units. They can be easily inserted, tested, modified, and retested.

In order to determine the validity of the similarity laws, large-scale modeling of a laminar-air proportional amplifier has been performed. The model is 10 times larger than the air device. Dynamic similarity between the large-scale model and the laminar-flow air device is obtained by equating the Reynolds number based on flow ($Q/w\nu$) through the power-jet nozzle of the large model to the Reynolds number based on flow through the power-jet nozzle of the actual device. Like performance characteristics were recorded for both the model and the air device. The characteristics were normalized with respect to power-jet chamber input states and the resulting model and air device curves were compared.

The versatility of the test facility is demonstrated by the fact that it is being used to refine an analytical control-volume model of the laminar proportional amplifier. It should also prove useful in research that is oriented toward the improvement of proportional amplifier performance and the investigations of other laminar flueric devices.

2. SIMILARITY AND MODELING

For similarity to exist between model and air device there must be geometric and kinematic similarity. Geometric similarity implies that the ratios of corresponding lengths in the model and air device are the same. Kinematic similarity exists when the ratios of corresponding velocities and accelerations are the same at corresponding points through the flow in model and air device. For geometric and kinematic similarity to exist simultaneously between model and air device, the dimensionless form of each physical variable must have the same value at corresponding points in the flow fields. Forces acting on corresponding fluid masses must be related by dimensionless ratios dependent on inertia, static pressure, viscosity, gravity, elasticity, heat conduction, and surfact tension effects.

When dealing with laminar flow, many of the forces are considered negligible. If the velocity of air flow is low, the fluid is essentially incompressible and thus the elasticity (compressibility) forces are negligible. Also if static pressure forces, gravity, heat conduction, and surface tension forces are considered negligible. the result is that only viscous and inertia forces are dominant. In order to

maintain similarity of viscous and inertia forces between corresponding fluid masses of the model and air device, the Reynolds number of the model is made equal to that of the air device. Reynolds number similarity imposes no restrictions on the fluid that can be used in the model. The investigator can choose the fluid most advantageous to his modeling needs.

3. THE MODELING TEST FACILITY

The test facility developed for large-scale modeling of laminar flueric devices is pictured in figure 1 and shown schematically in figure 2. The principal elements of the facility are: a reservoir for storing the fluid for recirculation thrcugh the model, a centrifugal pump for pressurizing the three input lines to the test section, a model test section, three output lines from the model test section back to the reservoir, and an oil temperature controlling system.

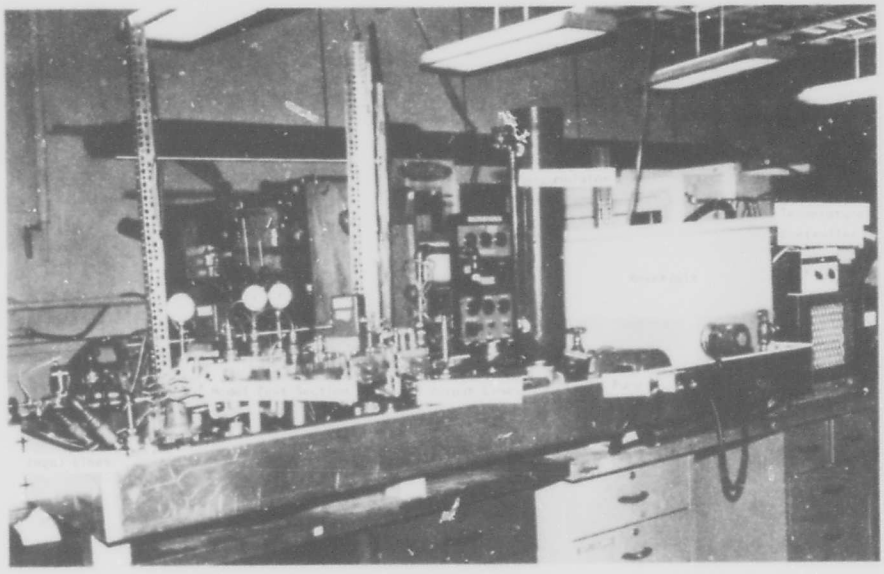

Figure 1. Silicone oil test apparatus.

An accumulator is located at the output of the pump to reduce pressure fluctuations caused by the pump impellers. Pressure fluctuations are reduced to less than one percent (peak to peak) of the total pressure at the inlet to the test section. A high-level and a low-level pressure regulator are provided for controlling input pressure to the three test-section inlets. The high-level regulator feeds one inlet while the low-level regulator feeds a proportioning valve which is connected to two low-level test-section inlets. The proportioning valve has rotary actuation, the actuator rotating 80° from left outlet wide open, right outlet shut, to right outlet wide open, left outlet shut. Figure 3 shows proportioning characteristics of this valve with a proportioning amplifier in the test section. Characteristics are given for power-jet pressure $P_+ = 55.1$ kPa. The low-level pressure regulator is set to drive the amplifier to saturation at $P_+ = 55.1$ kPa in taking both characteristics. The pressure difference across the two

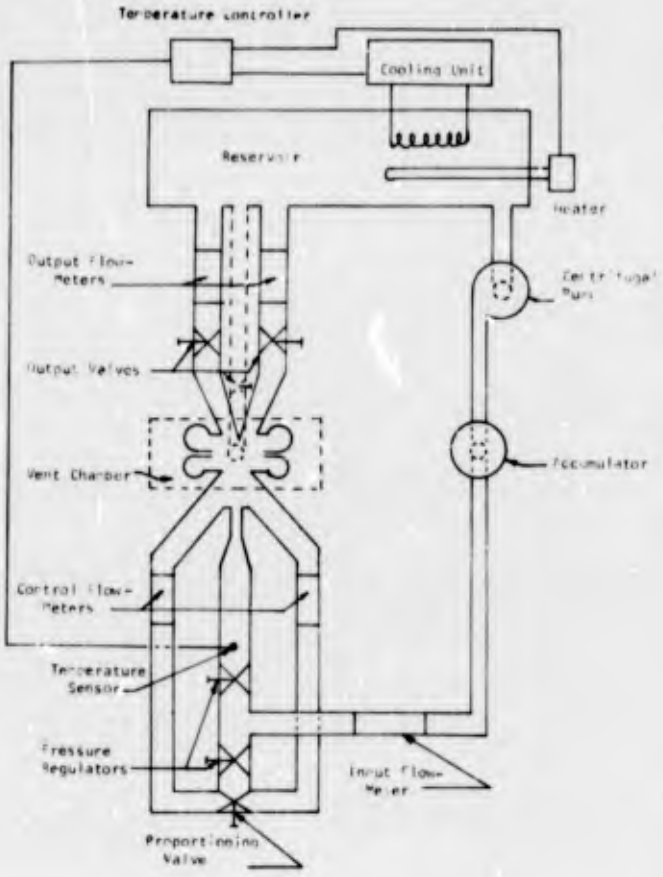

Figure 2. Silicone oil test stand schematic.

valve outlets (control channel inputs) is plotted versus the valve actuator setting. This valve is an inexpensive, readily available item. If a greater degree or linearity is desired, either a more sophisticated proportioning valve must be developed or a cam and gearing means attached to the present valve. Valves are at each of the outlets from the test section to control the output flow from the test model.

Flowmeters measure flow rates into and out of the test section. One high-level flowmeter measures the total flow rate to the test section. Two low-level flowmeters measure the flow rate to the two low-level inlets to the test section. Two additional flowmeters are located at two of the outlets from the test section to measure the output flow.

Flowmeters are of the laminar-flow, straight, smooth-pipe type. Two pressure taps are on each of the flowmeters for measurement of the pressure drop along a fixed length of each pipe. The flowmeters are calibrated by timing the collection of fluid in a graduated container while recording the pressure drop along the flowmetering section. Flowmeter calibration curves are given in figure 4. These flowmeters were designed for the flow rates encountered in the test model using the fluid selected for modeling validation. If a substantially different model or a fluid with different properties were to be used, suitable flowmeters could be readily substituted.

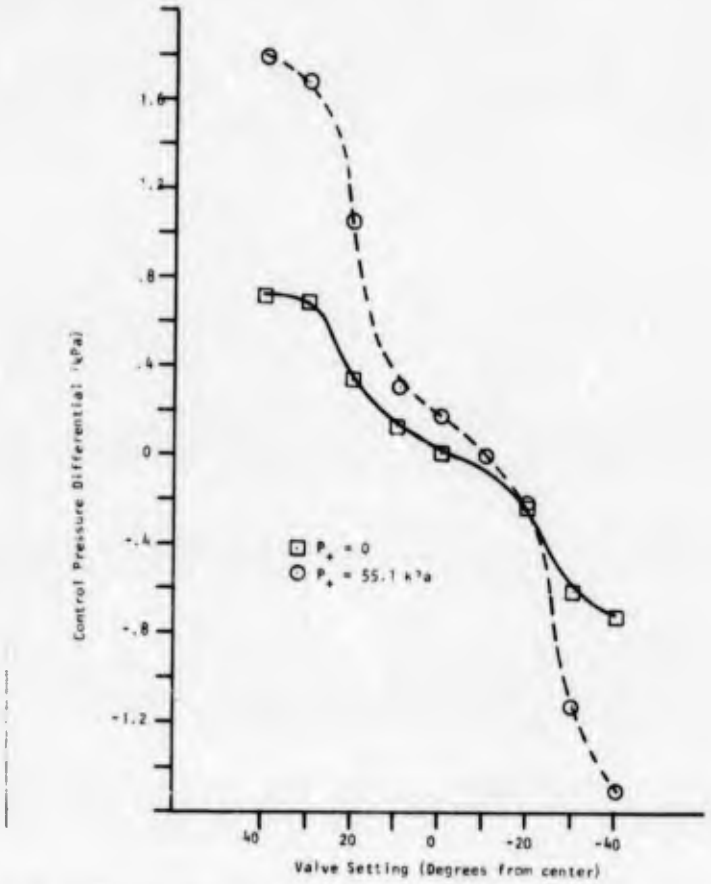

Figure 3. Control pressure differential vs proportional valve setting.

4. SELECTION OF GEOMETRIC SCALING FACTOR AND MODEL WORKING FLUID

An existing laminar proportional amplifier was selected as the air device for investigating the validity of large scale modeling with the test facility. Ten-to-one was chose as the geometrical scaling factor between model and air device. This scaling factor results in a model large enough to investigate the internal flow phenomena without significant interference with the flow.

Silicone oil with a kinematic viscosity of 5.0×10^{-5} m^2/s (50 centistokes) at 25°C was chosen as fluid for the model. The choice of this relatively high-viscosity oil allows one to operate the model at pressures that are easily measureable (approximately 85 times higher than those encountered in the air device. Another advantage of silicone oil is that it does not react with most materials and its properties are stable for long periods. The viscosity is not affected by shear rates encountered in the model operating under normal working conditions.

The oil viscosity changes with temperature, therefore, special care must be taken to maintain a constant temperature of the working fluid when performing tests. A thermostatically controlled cooling and heating system is used to maintain a constant oil temperature during testing. This system, shown schematically in fig. 2, is capable of maintaining the oil temperature in the test section during test to ±0.1°C.

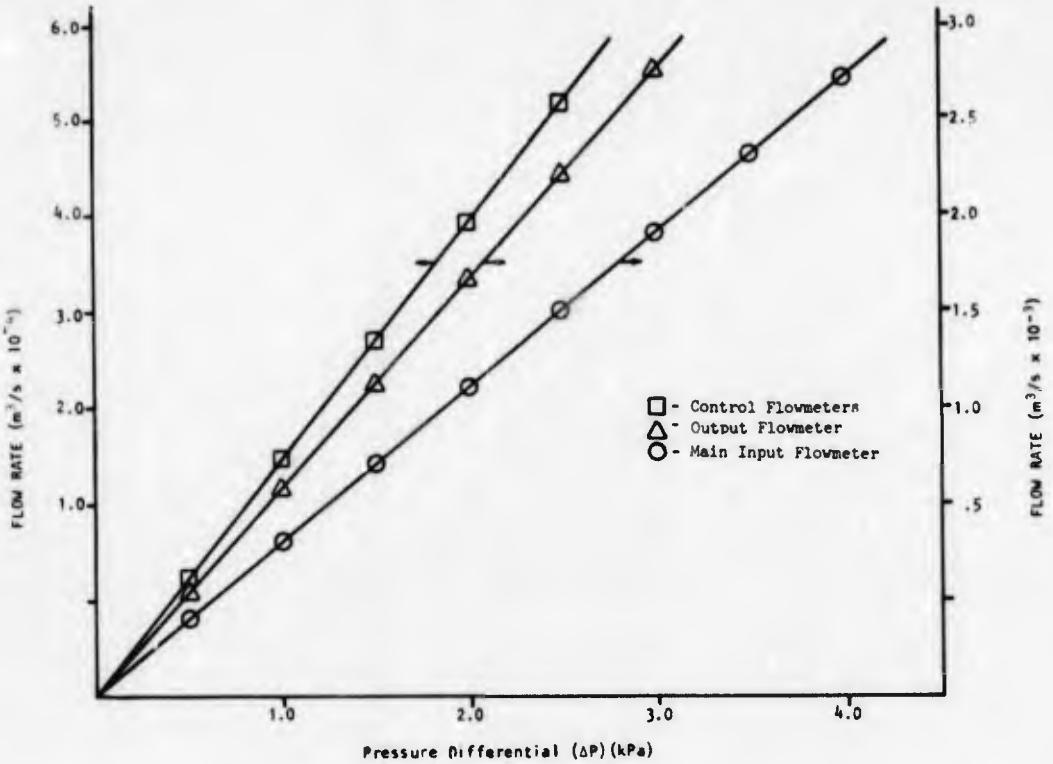

Figure 4. Flowmeter calibrating curves.

Figure 5 is a graph of kinematic viscosity of the silicone oil, used in the modeling facility, and of air as a function of temperature. The oil graph is extracted from information supplied with the oil from the Dow Corning Corporation (ref 1) while the air graph for temperatures of -20°C and higher is extracted from data given in reference 2. The air curve below -20°C is extrapolated from the data in ref 2. A comparison of the slopes of the oil and air curves shows that the viscosity of oil varies considerably more with temperature than does the viscosity of air. Thus, small temperature variations with oil may be used to advantage to simulate viscosity variations obtained only with great temperature differences in air. The effect on laminar-air unit characteristics caused by a variation in fluid viscosity may be simulated by using silicone oil and changing its viscosity by heating or cooling the ambient oil. The oil temperature range in the vicinity of 25°C that results in the same vicosity range as air over the military specifications temperature range of -54° to 74°C (-65° to 165°F) is 53° to 11°C. By varying the required temperature on the temperature controller, the oil test rig may be used to simulate viscosity variation in the operating temperature range of laminar units for use in military hardware.

---

[1]Anon., Information About Silicone Fluid Products, Dow Corning Corporation Midland, Bulletin: 05-183, Michigan, August 1967.

[2]Schlichting, H., Boundary Layer Theory, 4th Edition, McGraw-Hill Book Company, Inc., New York, 1960 p. 8

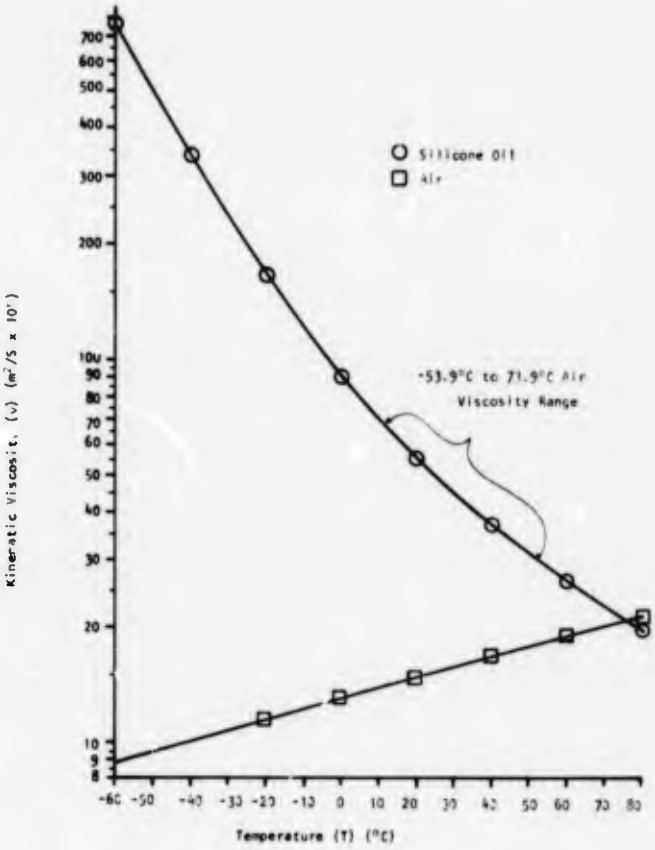

Figure 5. Kinematic viscosity of silicone oil and air vs temperature.

5. TEST UNITS

Figure 6 is a silhouette of the proportional amplifier designed to use air as its working fluid. It has a power-jet nozzle width of .102 cm and a depth of .0503 cm, yielding an aspect ratio h/w of .495. The large-scale model utilizing silicone oil has a power-jet nozzle width of 1.016 cm and a depth of .508 cm with an aspect ratio of .5. Both the air unit and the oil model were machined on an optically-controlled milling machine using the same line drawing. Critical dimensions of the interaction regions on the plan view of the oil model deviated by 2 percent or less from similar dimensions of the air device when scaled up by a factor of 10.

Because the oil model utilizes a vent chamber and pipe leading to the reservoir, a similar arrangement was added to the air model to obtain similarity. Due to fabrication considerations, where the vent pipe on the oil test rig has one right angle bend and a capped tee on the line, the vent pipe on the air unit is straight. The lengths and diameters of both vent tubes are geometrically similar, however.

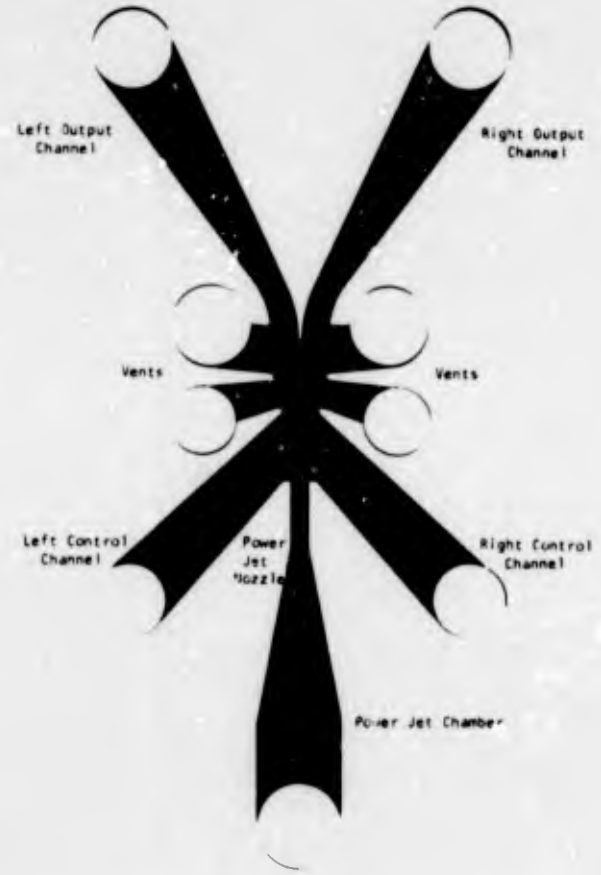

Figure 6. Proportional amplifier silhouette.

6. MODELING TESTS

Proportional amplifier performance characteristics were recorded for the oil model and air device at seven Reynolds numbers, (350 to 650) based on flow, over the operating range of the amplifiers in order to test modeling validity. These characteristics included power-jet nozzle discharge coefficient, pressure gain, control-input impedance, and output impedance. Reynolds numbers were determined from measurement of input power-jet flow and corresponding power-jet pressures recorded over the operating range of each unit. Using the air-unit data, Reynolds numbers based on flow, N_{R_Q}, were computed for seven points over the unit's operating range using the following formula

$$N_{R_Q} = \frac{\frac{Q}{A} \times h}{\nu} = \frac{Q}{w\nu}$$

where

A = cross-sectional area of nozzle

h = depth of nozzle

w = width of nozzle

Q = measured volumetric flow rate through nozzle

ν = kinematic viscosity

The choice of nozzle depth (h) as the characteristic dimension for determination of Reynolds number is based on investigations on laminar-jet proportional amplifiers conducted by Manion and Mon (ref 3). Data obtained during the investigations indicated that channel depth rather than depth squared is a better choice for the characteristic dimension since the essential parts of the flow field (in the power-jet nozzle) are not fully developed in the depth dimension over the design operating range of the amplifier.

Using the relationship for N_{RQ} and the power-jet flow versus input-pressure curve for the oil model, power-jet pressures required to yield equivalent Reynolds numbers for the oil model were determined. These Reynolds numbers, given in table I for the air unit and table II for the oil model were used in measuring performance characteristics of the model and air device.

6.1 Method of Measurement

During compilation of data in this report every attempt was made to use the most accurate instrumentation. Data were recorded on an X-Y plotter with the pressure drop corresponding to flow rates and pressures sensed with precision electronic transducers. Scales of the X and Y coordinates were calibrated with a manometer or pressure gage accurate to within 1 percent of full scale. The linear dimensions of the air unit were measured with a machinist's microscope with X and Y micrometer scales and with a micrometer depth gage. Corresponding oil-model dimensions were measured with a scale and a micrometer depth gage directly from the unit. The error of these measurements was estimated to be 1 percent.

The Reynolds number based on flow through the power-jet was determined experimentally by measuring flow rate through the nozzle height and width of the nozzle and the kinematic viscosity of the oil. An independent viscosity measurement of the oil was made at room temperature (25°C) with a viscometer which is accurate to better than one percent of full scale. The measured value (50.1 centistokes) agreed with the corresponding point on the graph supplied with the oil. Due to lack of an accurate temperature bath, measurements at temperatures other than ambient could not be made with confidence.

The probable experimental error, $\varepsilon(N_{RQ})$, in determining N_{RQ}, $\frac{Q}{w\nu}$, can be estimated using the special rules for combining errors given in Beers (ref 4) by employing the following expression.

---

[3]Manion, F. M. and Mon, G., Fluerics: 33, Design and Staging of Laminar Proportional Amplifiers,

[4]Beers, Y., Introduction to the Theory of Error, Addison-Wesley Publishing Company, Inc., Reading Massachusetts, 1956, p. 34.

TABLE I

AIR PROPORTIONAL AMPLIFIER TEST DATA

Power-Jet Pressure (P_+) (kPa)	Power-Jet Flow Rate (Q_+) ($\frac{m^3}{s} \times 10^{-3}$)	Reynolds No. (Ideal Flow) (Re_p)	Reynolds No. (Re_Q)	Discharge Coefficient (C_D)
.244	5.40	680	350	.515
.296	6.18	749	400	.534
.356	6.95	822	450	.547
.425	7.72	899	500	.556
.496	8.50	970	550	.567
.566	9.27	1036	600	.579
.653	10.03	1112	650	.584

TABLE II

OIL PROPORTIONAL AMPLIFIER TEST DATA

Power-Jet Pressure (P_+) (kPa)	Power-Jet Flow Rate (Q_+) ($\frac{m^3}{s} \times 10^{-3}$)	Reynolds No. (Ideal Flow) (Re_p)	Reynolds No. (Re_Q)	Discharge Coefficient (C_D)
20.6	1.79	680	350	.515
25.4	2.04	751	400	.533
30.1	2.30	826	450	.545
36.4	2.56	897	500	.557
42.1	2.81	961	550	.572
48.8	3.07	1026	600	.585
54.8	3.32	1091	650	.596

$$\frac{\epsilon^{(N_{R_Q})}}{N_{R_Q}} = \left[\left(\frac{\epsilon(Q)}{Q}\right)^2 + \left(\frac{\epsilon(W)}{W}\right)^2 + \left(\frac{\epsilon(\nu)}{\nu}\right)^2\right]^{\frac{1}{2}}$$

where

$\epsilon(Q)$ = probable error in measuring flow rate
$\epsilon(\nu)$ = probable error in measuring viscosity
$\epsilon(W)$ = probable error in measuring nozzle width

If the probable percentage error in measuring flow rate is assumed to be 2 percent (which includes the flowmeter error and error in reading the flowmeter output), in viscosity less than 1 percent for oil and air, and in measuring nozzle width less than 1 percent, then these errors will lead to a probable error of less than 2.5 percent for N_{R_Q} for both oil model and air device.

6.2 Performance Characteristics

In tables I and II data are given on Reynolds numbers based on flow (N_{R_Q}), power-jet pressures, flow rates, Reynolds numbers based on power-jet pressure (N_{R_Q}) and nozzle-discharge coefficients (C_D). The method of computing Reynolds number based on power-jet pressure and nozzle-discharge coefficients follows.

Assuming ideal frictionless flow between the inlet to the power-jet chamber designed by subscript 1 and the nozzle exhaust designated by subscript 2, both of which are on the same plane, the Bernoulli equation may be written between these two points:

$$P_1 + \frac{1}{2}\rho V_1^2 = P_2 + \frac{1}{2}\rho V_2^2 = P_+$$

where

P = static pressure
P_+ = total pressure
ρ = density of fluid
V = velocity of flow

Supply pressure to the amplifier (P_+) is measured with a total pressure probe; i.e., normal to the incoming flow to the power-jet chamber; therefore, it is equal to the sum of the static pressure (P_2) and the dynamic pressure ($1/2\rho V_1^2$). The static pressure P_2 at the nozzle exit is assumed to be ambient pressure or zero. The velocity at the power-jet nozzle exit thus reduces to the following expression:

$$V_2 = \left(\frac{2P_+}{\rho}\right)^{\frac{1}{2}}$$

Substituting this value V_j in the expression for Reynolds number results in the following expression for Reynolds number based on P_+ assuming ideal flow (N_{R_P})

$$N_{R_P} = \frac{h}{\nu}\left(\frac{2P_+}{\rho}\right)^{\frac{1}{2}}$$

The nozzle discharge coefficient (C_D) is defined as the ratio of the actual measured flow rate (Q_+) through the power-jet nozzle to the idealized flow rate of a perfect fluid (Q_i). C_D is obtained using the following relationship:

$$C_D = \frac{Q_+}{Q_i} = \frac{Q_+}{AV_2} = \frac{Q_+}{A\left(\frac{2P_+}{\rho}\right)^{\frac{1}{2}}} = \frac{N_{R_Q} A \frac{\nu}{h}}{N_{R_P} A \frac{\nu}{h}} = \frac{N_{R_Q}}{N_{R_P}}$$

Figure 7 gives discharge coefficient versus Reynolds number based on flow rate for both the oil model and air device.

Figure 8 and 9 give pressure gain curves recorded for both the oil model and air device at three different Reynolds numbers. In figure 8 the oil-model data are reduced to air device scale by multiplying by the ratio of air device power-jet pressure to model power-jet pressure. In figure 9 the data for each case are normalized with respect to the power-jet pressure to each unit. Figure 8 allows comparison of the actual data while figure 9 brings out the effect of Reynolds number on gain characteristics. The data are generated by blocking one control and deflecting the power-jet to saturation by increasing the pressure to the opposite control while monitoring control and output pressure differentials. These curves are compared with matching zero points.

To further test the validity of the silicone oil model, input and output impedances were measured for both the model and the air unit over the same power-jet pressure range employed for the gain measurements. The input impedances of each control were measured separately. Control flow was introduced simultaneously through each control with both output channels blocked while maintaining the output pressure differential at zero. Following this procedure input control flow was recorded as a function of input control pressure for each leg. The control input impedance curves generated were relatively unaffected by variations in flow Reynolds number over the range tested. Figure 10 shows the input impedances of the right and left controls for the oil model and the air unit at $N_{RQ} = 500$. These curves are representative of similar curves recorded over the operating Reynolds number range of the units. Figure 11 shows the total control impedance curves for the same case. Here the normalized right and left control-flow rates for each unit are summed at equal normalized control pressures.

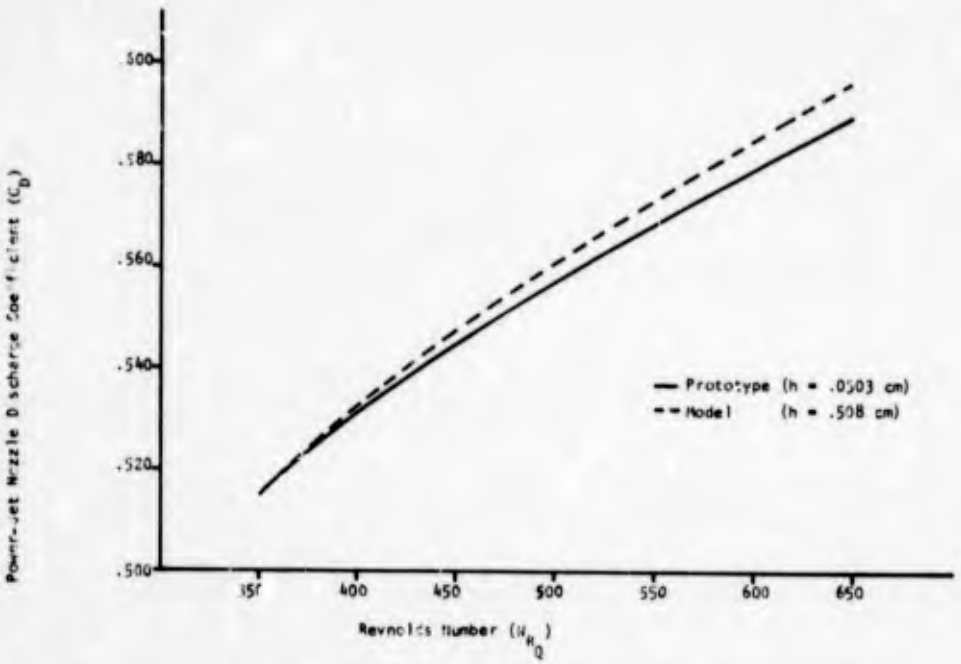

Figure 7. Power-jet nozzle discharge coefficient vs Reynolds number.

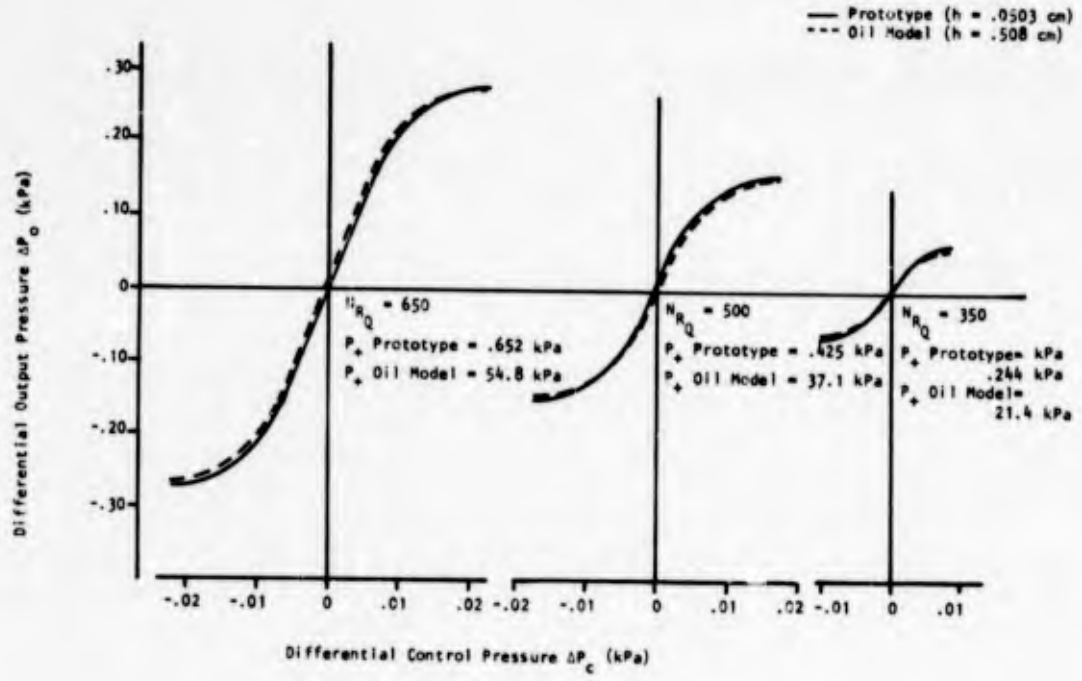

Figure 8. Pressure gain curves.

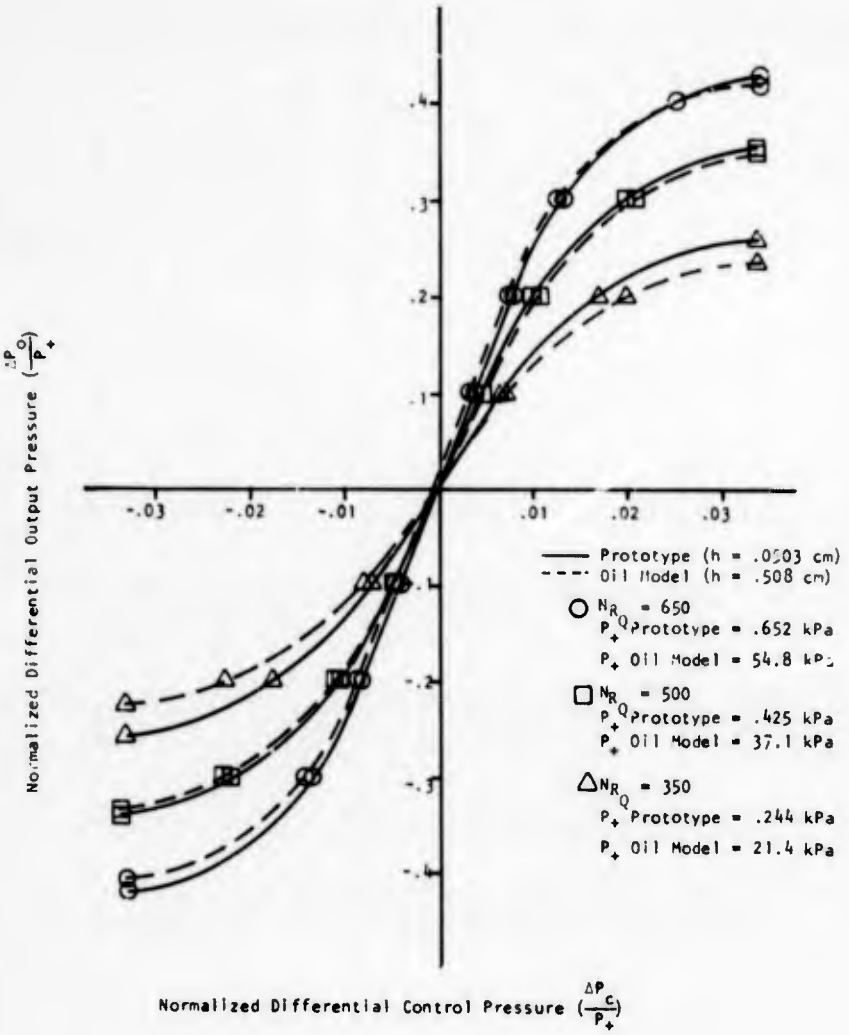

Figure 9. Normalized pressure gain curves.

Output impedance curves were recorded after deflection of the power-jet by one control only to yield maximum output pressure at the opposite receiver while driving the jet to saturation. Both outputs were initially blocked. The output to which the jet is directed is gradually opened as flow through this output is recorded as a function of pressure at the output. Output impedance data were recorded for both output legs of each amplifier at the same power-jet pressures used to obtain the control input impedances. Figure 12 gives left and right output impedance curves for the oil model and the air unit for the same Reynolds numbers. The model test data are converted to air device scale as were the gain data in figure 8. Figure 13 gives the average of the left and right output impedance of the model and the air device at the same Reynolds numbers. Pressure and flow values for these curves are normalized with respect to input pressure and flow rate respectively.

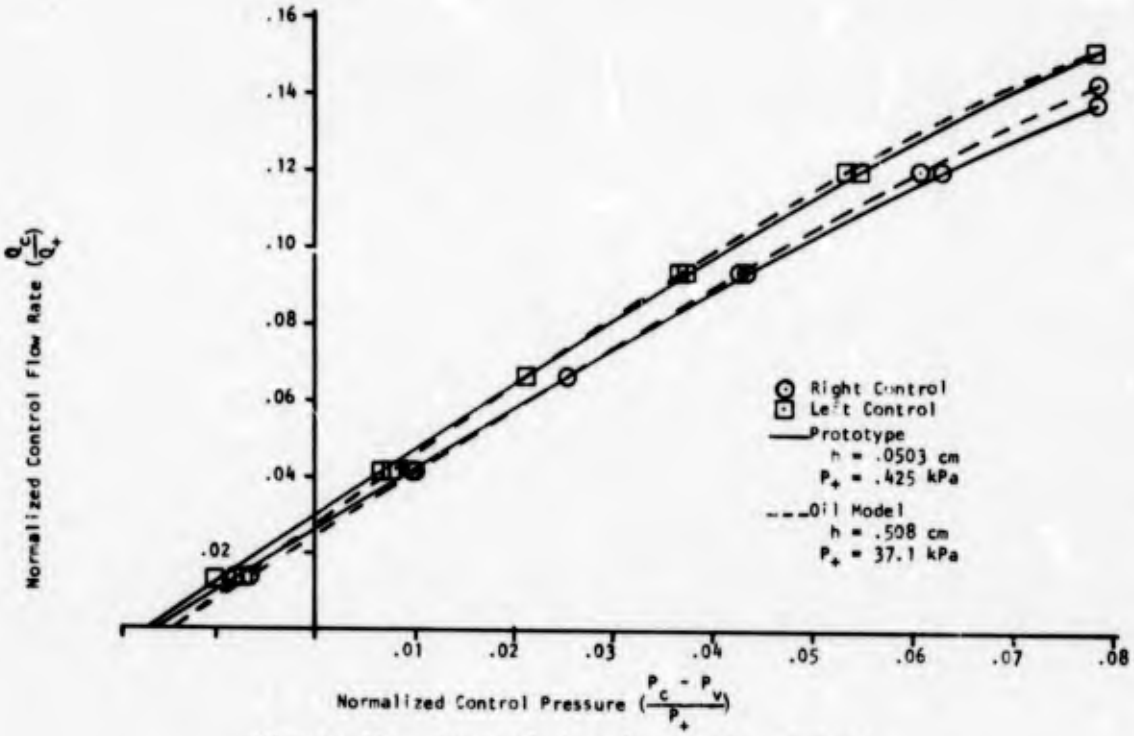

Figure 10. Control impedance (N_{RQ} = 500).

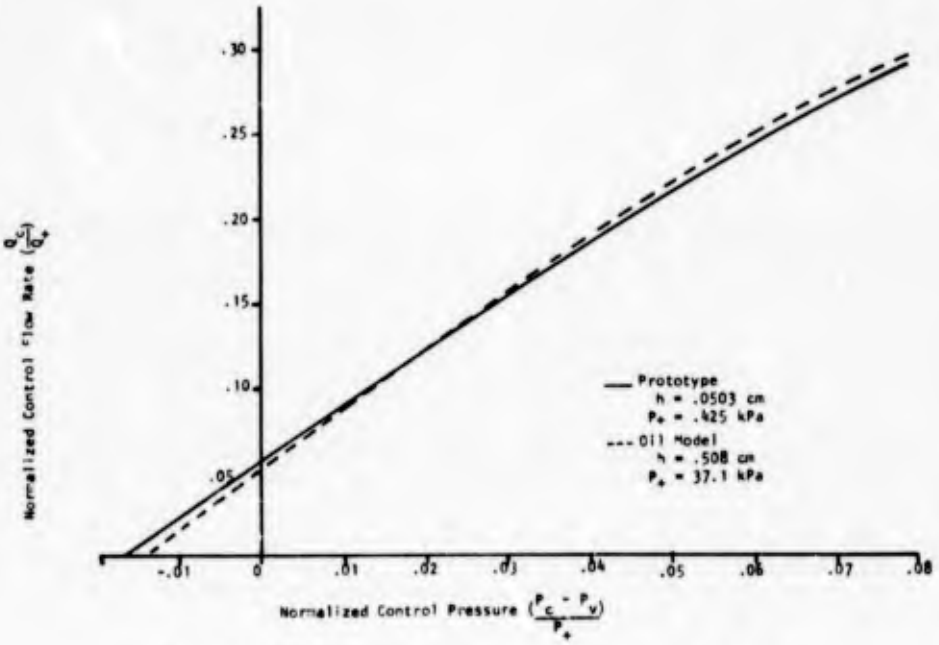

Figure 11. Control impedance (N_{RQ} = 500).

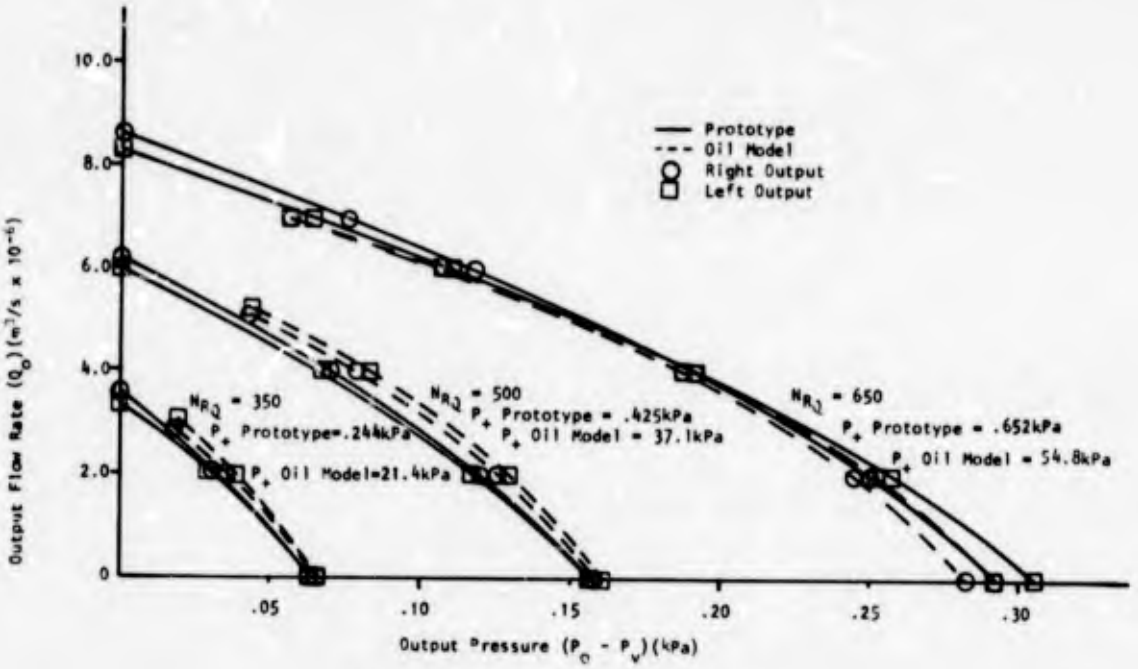

Figure 12. Output impedance.

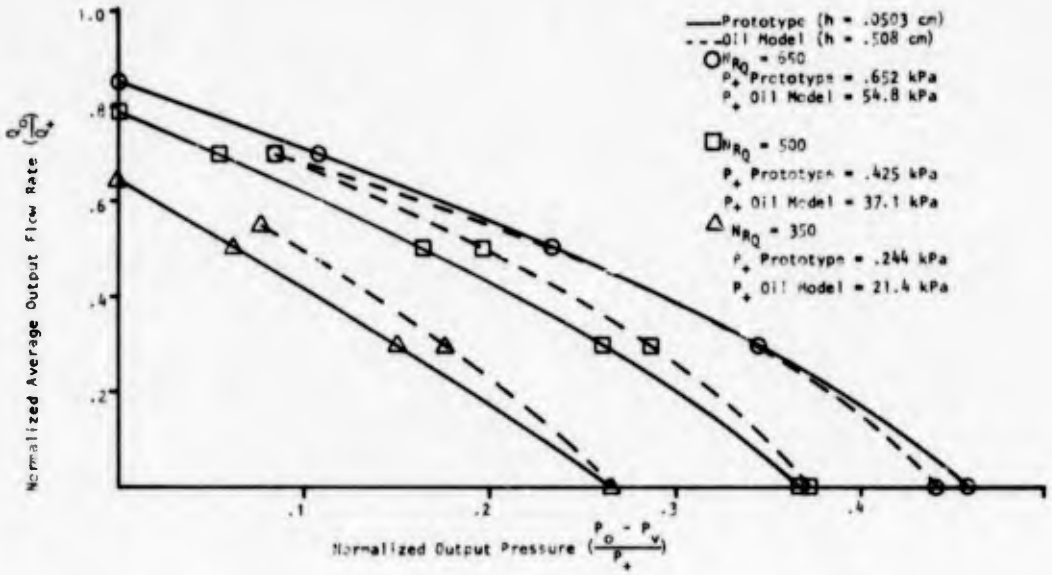

Figure 13. Normalized output impedance.

6.3 Comparison of Model and Air Device Performance Characteristics

Comparing values of discharge coefficients for the air and oil units, given in figure 7, it is seen that values for the air unit are from 0 to 2 percent lower than those at the same Reynolds numbers (N_{RQ}) for the oil model. This agreement is well within the deviation that would be expected due to the existence of experimental error in determining the various Reynolds numbers. This fact would also indicate that the experimental error is lower than anticipated.

Referring to the pressure gain curves (figs. 8 and 9) it is observed that there is close agreement between the normalized oil-model gain curves and the corresponding air-unit curves. Differences between measurements of model and air-unit pressure gains in the linear region for corresponding Reynolds numbers vary from 0 to 10 percent, with differences increasing with decreasing Reynolds number. Differential output pressure agreement was within 2 to 9 percent over the Reynolds number range, with greater differences encountered in the lower Reynolds number cases.

These differences may be accounted for in part by the existence of deviations of up to 2 percent from similarity between critical dimensions of the interaction regions of the amplifiers. The fact that modeling agreement for this case decreases with decreasing Reynolds number is probably due to an increase in power-jet lateral spreading along the direction off jet flow, as well as an increase in the three-dimensionality of the flow with a decrease in Reynolds number. This would tend to accentuate the influence on performance characteristics of channel boudaries bordering the interaction region of each amplifier. Thus, the dissimilarities which exist in the interaction region of the air device and the model would tend to have more effect on amplifier performance characteristics with decreasing Reynolds number.

These points can be better appreciated by observing figures 14 to 19 which are photographs of a water visualization model with the same dimensions as the oil model. In this model small dye streams are injected into the lateral boundaries of the power jet stream of the power-jet nozzle. The boundary stream lines bordering the power jet which issue into a clear interaction region can thus be visualized and photographed. Figures 14 through 16 show mid-plane stream lines while figures 17 through 19 show jet-boundary stream lines along a plane near the bottom plate. The photos show clearly the jet spreading at three different Reynolds numbers (N_{RQ}) 650, 500 and 350, respectively. These photographs were taken with the amplifier control and output channels blocked. As was stated in the previous discussion it is readily observed from the photographs that lateral-jet spreading increases and power-jet flow becomes more three-dimensional with decreasing Reynolds number. Power-jet flow thus comes more under the influence of the downstream lips of the control channels, as well as other physical boundaries of the interactions region, thus resulting in a greater effect on performance characteristics by these boundaries.

It is observed that both the left and the right control impedance curves of the oil model are in good agreement with the corresponding air device curves. In fact, there is a greater difference between the left and right control impedances for each individual unit than there is between the corresponding model and air device curves. This is because both units have approximately the same internal mechanical

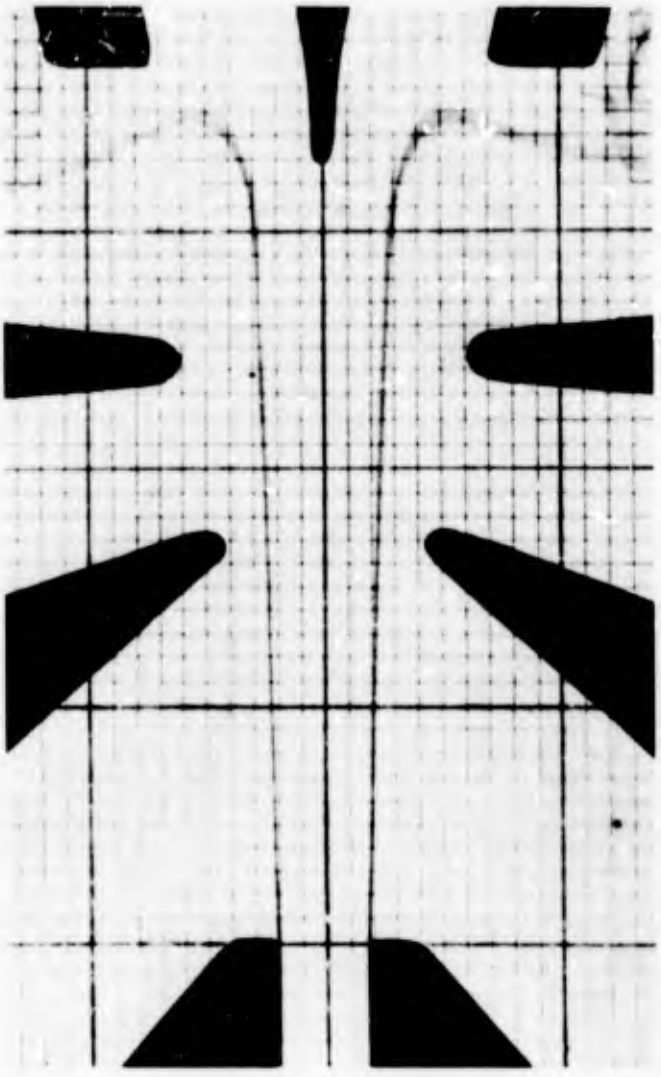

Figure 14. Power-jet (N_{R_Q} = 650) showing mid-plane jet-edge streamlines.

bias, indicating the high degree of similarity that exists. Figure 11 shows the total control input impedance curves for the same case. Again, as for the individual input impedance curves, agreement is good. The difference in the slopes varies between 0 to 7 percent.

Figure 12 gives left and right output impedance curves for the oil model and air unit for three Reynolds numbers. Here also, as for the control impedance data, the right and left impedance curves for each unit at each Reynolds number vary, but not to the extent observed for input impedance. Agreement between model and air device curves is good, being very good for the higher Reynolds number case and decreasing with decreasing Reynolds number. This can be seen more clearly from the normalized average output data presented in figure 13. The deterioration in agreement with decreasing Reynolds number, might be accounted for in the same manner as a similar deterioration of gain curve agreement, explained earlier.

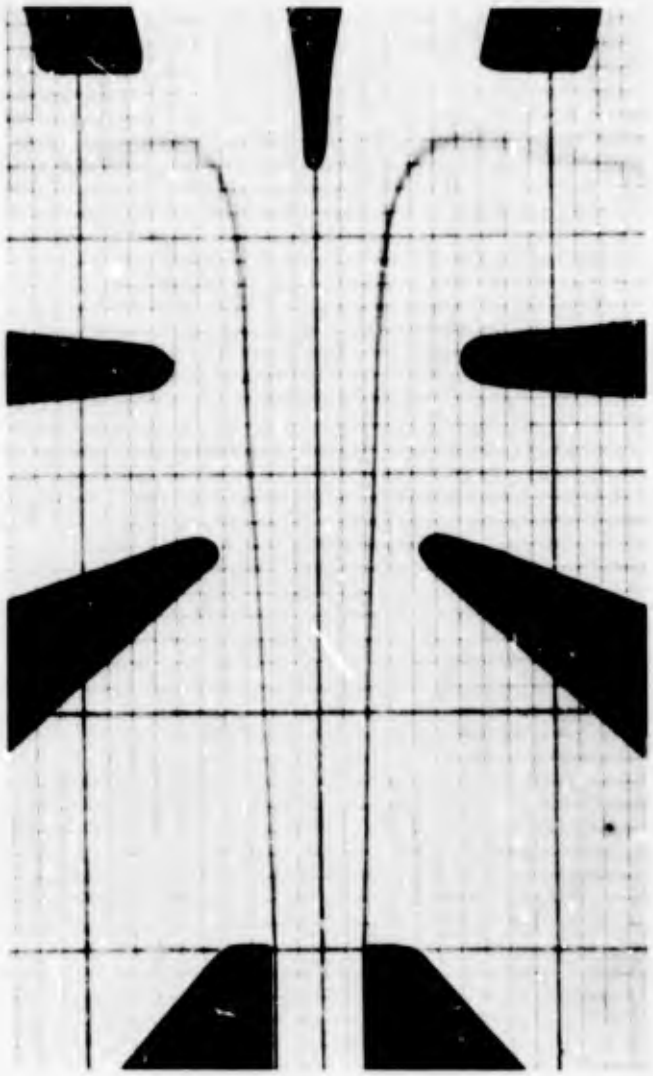

Figure 15. Power-jet (N_{RQ} = 500) showing mid-plane jet-edge streamlines.

7. CONCLUSIONS

A test facility was designed, constructed and instrumented for use in large-scale modeling of laminar flueric flow phenomena; it is inexpensive and easy to operate. Models can be readily inserted, tested and removed for modification. Using Reynolds number based on flow as the modeling parameter, static performance characteristics of a large-scale model were compared to those of an air device. Agreement between similar amplifier performance characteristics was very good. Differences between normalized model and air device characteristics appear to be within limits of expected experimental error. Results obtained thus verify that the laws of similitude are valid for the conditions specified, and can be readily used. Modeling of flueric element dynamic characteristics was not investigated but is planned for the future.

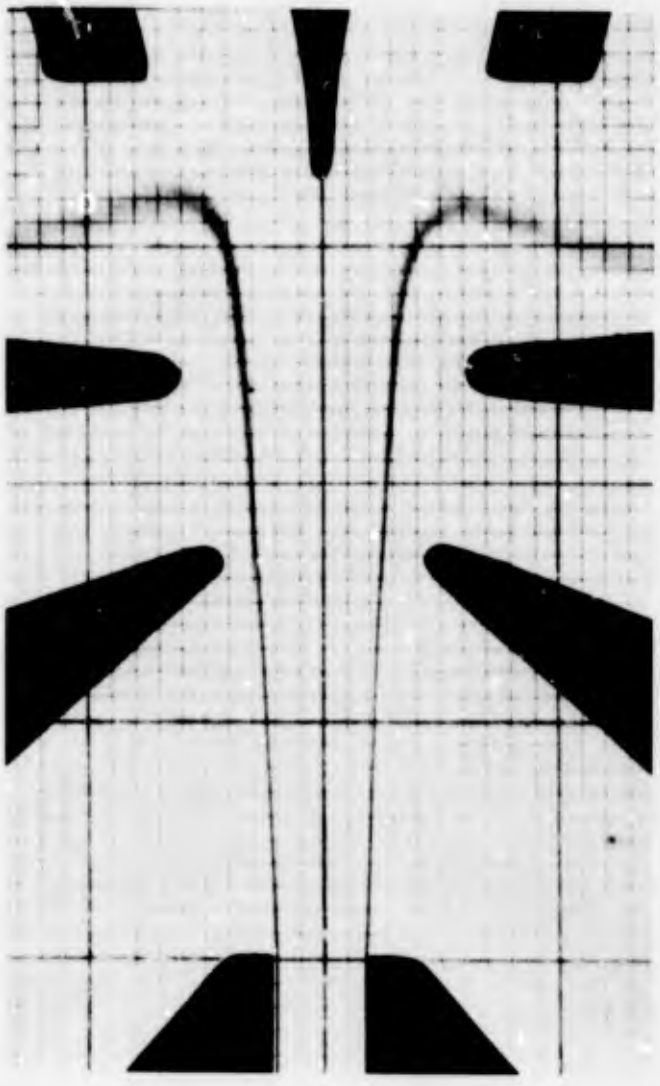

Figure 16. Power-jet (N_{RQ} = 350) showing mid-plane jet-edge streamlines.

The good quantitative agreement between model and air device characteristics and the flexibility and ease of operation of the modeling facility, should make it an invaluable tool in quantitative investigation of internal flow fields of laminar flueric devices. In devices where slight dimensional variations are critical to unit performance, use of large-scale modeling will allow more precise control of critical dimensions and thus an accurate determination of the effect on unit performance caused by dimensional variations. Investigation of the internal flow fields in these and other areas should assist investigators in their understanding of the flow phenomena in laminar flueric devices and thus in improving unit performance.

The test facility is currently being used for static surface pressure mapping of a proportional amplifier of the type used as the model for this report. Internal flow-field measurements and refinement of the analytical control-volume model of the laminar-proportional amplifier are planned for the future.

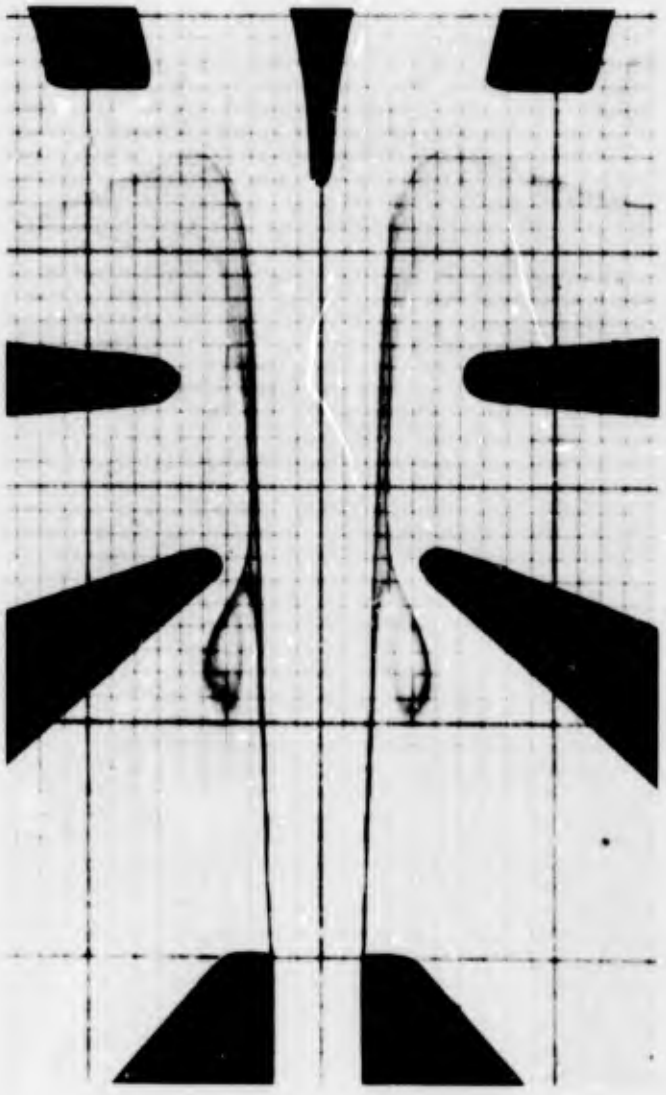

Figure 17. Power-jet (N_{R_Q} = 650) showing base jet-edge streamlines.

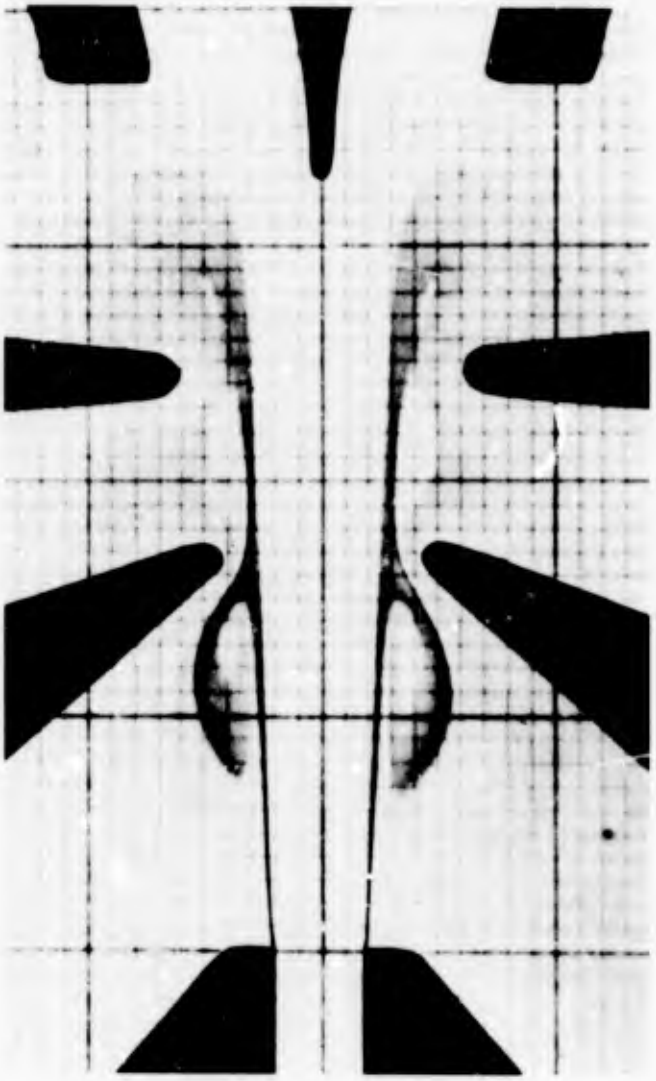

Figure 18. Power-jet (N_{RQ} = 500) showing base jet-edge streamlines.

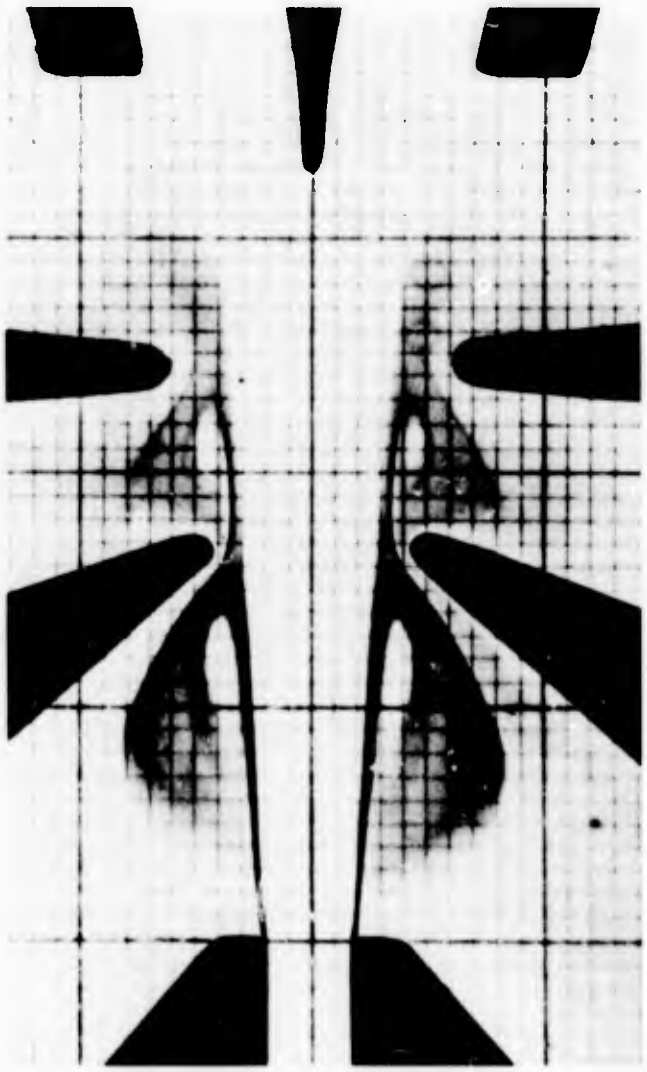

Figure 19. Power-jet (N_{R_Q}) showing base jet-edge streamlines.

LIST OF SYMBOLS

A - power-jet nozzle area, (m^2)

C_D - power-jet nozzle discharge coefficient

G_p - pressure gain

h - power-jet nozzle height (m)

P_+ - supply pressure, (kPa)

P_1 - static pressure at inlet to power-jet chamber, (kPa)

P_2 - static pressure at power-jet nozzle exit, (kPa)

Pc - control pressure, (kPa)

P_o - output pressure, (kPa)

Q_+ - supply flow rate, (m^3/s)

Qc - control flow rate, (m^3/s)

Qi - supply flow rate assuming ideal flow, (m^3/s)

Qo - output flow rate, (m^3/s)

N_{R_P} - Reynolds number assuming ideal flow

N_{R_Q} - Reynolds number based on power-jet flow rate

V - average velocity, (m/s)

w - power-jet nozzle width, (m)

$\varepsilon(Q)$ - error in measuring flow rate, (m^3/s)

$\varepsilon(w)$ - error in measuring power-jet nozzle width, (m^2)

$\varepsilon(\nu)$ - error in measuring kinematic viscosity, (m^2/s)

ν - kinematic viscosity, (m^2/s)

ρ - density of fluid, (kg/m^3)